Computer-aid drug design, synthesis, and anticoagulant activity evaluation of novel dabigatran derivatives as thrombin inhibitors

Shanshan Huang, Yujie Ren, Xiuxiu Peng, Pingping Qian, Lingwei Meng

PII: S0928-0987(19)30228-3
DOI: https://doi.org/10.1016/j.ejps.2019.104965
Article Number: 104965
Reference: PHASCI 104965

To appear in: *European Journal of Pharmaceutical Sciences*

Received date: 15 April 2019
Revised date: 3 June 2019
Accepted date: 20 June 2019

Please cite this article as: S. Huang, Y. Ren, X. Peng, et al., Computer-aid drug design, synthesis, and anticoagulant activity evaluation of novel dabigatran derivatives as thrombin inhibitors, European Journal of Pharmaceutical Sciences, https://doi.org/10.1016/j.ejps.2019.104965

Computer-aid Drug Design, Synthesis, and Anticoagulant Activity Evaluation of Novel Dabigatran Derivatives as Thrombin Inhibitors

Shanshan Huang, Yujie Ren*, Xiuxiu Peng, Pingping Qian and Lingwei Meng
College of Chemical and Environmental Engineering, Shanghai Institute of Technology, 100 Haiquan Road, Shanghai 201418, China.
***Correspondence:** Yujie Ren,
E-mail: clab@sit.edu.cn
Tel.: +021-60877231

Abstract: In this study, computer-aided drug design techniques were adopted to explore the structural and chemical features for dabigatran and design novel derivatives. The built 3D-QSAR models demonstrated significant statistical quality and excellent predictive ability by internal and external validation. Based on QSAR information, 11 novel dabigatran derivatives (12a-12k) were designed and predicted, then ADME prediction and molecular docking were performed. Furthermore, all designed compounds were synthesized and characterized by ^{1}H NMR, ^{13}C NMR and HR-MS. Finally, they were evaluated for anticoagulant activity in vitro. The activity results showed that the 10 obtained compounds exhibited comparable activity to the reference dabigatran ((IC_{50} = 9.99 ±1.48 nM), except for compound 12i. Further analysis on molecular docking was performed on three compounds (12a, 12c and 12g) with better activity (IC_{50} = 11.19 ±1.70 nM, IC_{50} = 10.94 ± 1.85 nM and IC_{50} = 11.19 ±1.70 nM). MD simulations (10 ns) were carried out, and their binding free energies were calculated, which showed strong hydrogen bond and pi–pi stacking interactions with key residues Gly219, Asp189 and Trp60D. The 10 novel dabigatran derivatives obtained can be further studied as anticoagulant candidate compounds.

Key words: Computer-aided drug design; dabigatran derivatives; synthesis; anticoagulant activity

1. Introduction

Cardiovascular diseases (CVDs) are the leading causes of mortality and morbidity worldwide. According to the World Health Organization, CVD mortality may be expected to reach about 25 million by 2030(Chaudhari et al., 2014). Thrombin, a multifunctional serine protease, is an important effector protease in CVD processes(Ahmad and Lip, 2012). Thrombin exhibits procoagulant and anticoagulant

properties in the blood coagulation cascade(De Candia, 2012). It activates platelets and catalyzes the conversion of fibrinogen to fibrin, which promotes the stability of blood clots and causes the blood to coagulate(B. et al., 2007). Therefore, thrombin is an important target in the treatment of CVDs.

To date, several thrombin inhibitors, including indirect thrombin inhibitors and direct thrombin inhibitors (DTIs), have been developed. DTIs with high specificity for thrombin have been the focus of anticoagulant drug development(Kam et al., 2005; Lee and Ansell, 2011). Several direct thrombin inhibitors (Figure 1), such as Ximelagatran(Gustafsson et al., 1998), Apixaban(Curto and Albaladejo, 2016), Argatroban(Berry et al., 1994) and Dabigatran etexilate(Eriksson et al., 2008), have been reported. Ximelagatrans is the first oral DIT and has significant inhibitory effect on thrombin in clinical. Later, ximelagatran was withdrawn from the market because it causes increased hepatic enzyme levels(WEITZ and BATES, 2005). Apixaban can significantly reduce the risk of thromboembolic disease. But it also increase the risk of anemia, bleeding and other adverse reactions(Granger et al., 2011). Argatroban is the first clinical direct thrombin inhibitor (DTI). However, after oral administration, it becomes unstable or even inactivated in the human body(Kim et al., 2015). Thus, dabigatran etexilate became the only orally available DTI in the market. In March 2008, the use of dabigatran etexilate for the prevention of venous thromboembolic events for patients who had undergone total hip and knee replacement surgery was approved by the European Medicines Administration(Eriksson et al., 2008). Dabigatran etexilate has been used to prevent stroke among patients with atrial fibrillation in phase III trials(Savelieva and Camm, 2014). Unlike other anticoagulants, dabigatran etexilate has several advantages, such as a wide therapeutic window, a fixed dose without monitoring

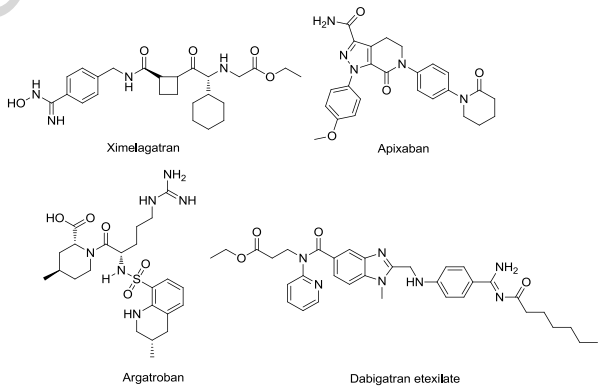

Figure 1. Chemical structures of some known thrombin inhibitors.

and less drug-drug interactions(Blommel and Blommel, 2011; Dahl, 2008; Sanford and Plosker, 2008). However, there are still unavoidable high-dose bleeding risks and expensive drawbacks(Haas, 2008; Pollack et al., 2015). In 2015, the monoclonal antibody Idarucizumab was approved for market in the United States. Idarucizumab can rapidly and safely reverse the anticoagulant effect to control the bleeding risk caused by dabigatran etexilate(Traynor, 2015). Still, dabigatran etexilate cannot be accepted by most patients because of its relatively high price caused by the patent protection and complex synthesis process. Therefore, it is meaningful to find new thrombin inhibitors with comparable activity to the dabigatran for preventing and treating CVDs.

Computer-aided drug design (CADD) is extensively applied in drug design. As a powerful design tool, CADD can improve the success rate of drug research and development (R&D), reduce R & D costs and shorten the R&D cycle. The approach has accelerated the lead optimization process by studying 3D features of chemicals(Huang et al., 2019). 3D-QSAR tools have been successfully applied in the discovery of inhibitors, such as HO-1 inhibitors(Amata et al., 2017), 5-lipoxygenase inhibitors(Ul-Haq et al., 2016) and antiviral drugs(Tu et al., 2017). In this work, based on the compounds and activities obtained from our previous work(Ren et al., 2016; Wang et al., 2016; Yang et al., 2017), the appropriate groups were introduced to design novel dabigatran derivatives from the aspects of QSAR information and chemical properties. The flow of this study are shown in Figure 2.

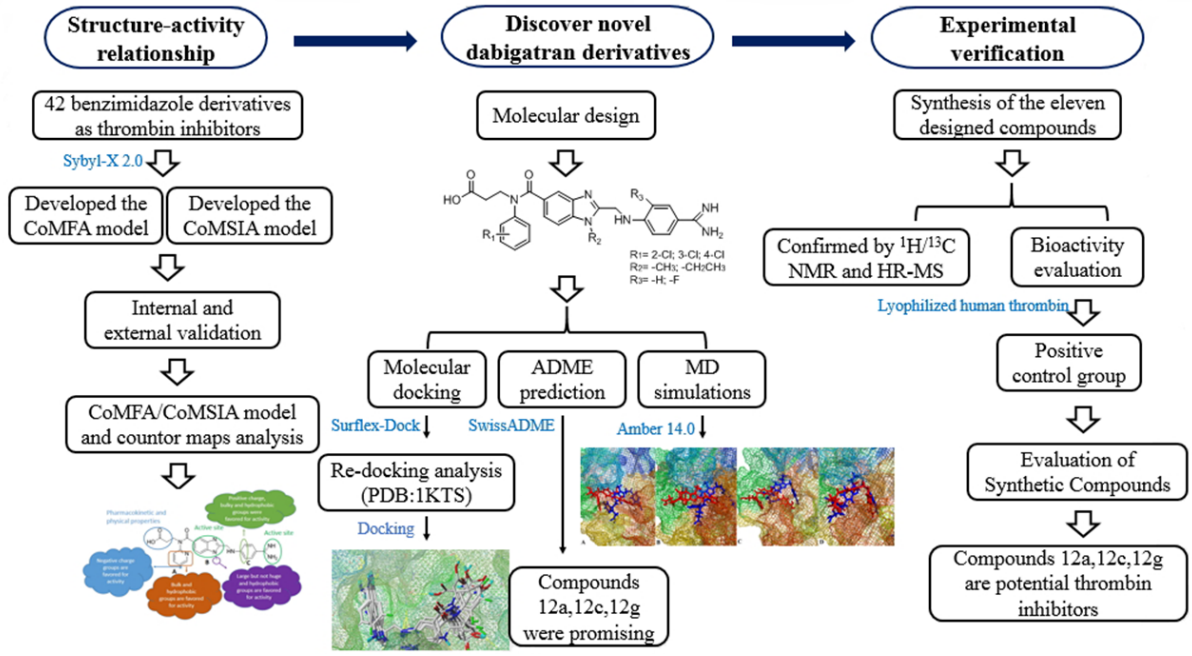

Figure 2. Flowchart of the study for the discovery of novel dabigatran derivatives

The above results lay an important foundation for the discovery of new anticoagulant candidates, and methods combining theory with practice can also provide the reference for the discovery of other drugs.

2. Results and discussion

2.1 Analysis of CoMFA and CoMSIA

The statistical results for the CoMFA and CoMSIA models were summarized in Table 1. In the CoMFA model, the PLS regression analysis obtained the q^2 of 0.705 and the ONC of 8. Then, the non-cross validation gave the satisfactory r^2 of 0.971 with the SEE of 0.090 and the F-statistic value of 114.648. The contributions of steric and electrostatic fields to the CoMFA model were 31.1% and 68.9%, respectively. In the CoMSIA model, the PLS regression analysis showed the q^2 of 0.707, the ONC of 10, the r^2 of 0.966, the SEE of 0.102 and the F value of 71.471. The contributions of steric, electrostatic, hydrophobic, H-bond acceptor and H-bond donor fields were 11.2%, 36.4%, 26.7%, 9.6% and 16.2%, respectively. It can be found that the electrostatic and hydrophobic field made major contributions among the five fields. As listed in Table 1, the r^2_{pred} value of CoMFA was 0.722 and the CoMSIA r^2_{pred} value was 0.699. The CoMFA R^2 value was 0.704 and the CoMSIA R^2 value was 0.790. The slopes k values (1.000 for CoMFA, 1.004 for CoMSIA) were both close to 1. R_0^2 values (0.756 for CoMFA, 0.881 for CoMSIA) were both close to R^2 values. For the CoMFA and CoMSIA model, the r_m^2 values were 0.544 and 0.552, the $(R^2-R_0^2)/R^2$ values were

Table 1. The statistical results of 3D-QSAR models

Parameter	CoMFA	CoMSIA
q^2	0.705	0.707
ONC	8	10
r^2	0.971	0.966
SEE	0.090	0.102
F	114.648	71.471
R_{pred}^2	0.722	0.699
R	0.839	0.889
R^2	0.704	0.790
k	1.000	1.004
R_0^2	0.756	0.881
r_m^2	0.544	0.552
$(R^2-R_0^2)/R^2$	-0.074	-0.115
MAE_{Test}	0.107	0.098

-0.074 and -0.115, respectively. The MAE_{text} values (0.107 for CoMFA, 0.098 for CoMSIA) were both less than the 0.1 × training set range (0.215). All the internal and external validation parameters of 3D-QSAR models were in an acceptable limit. The plots showing the actual and predicted pIC_{50} values for the total set in the CoMFA and CoMSIA approaches were represented in Figure 3. Most points were evenly distributed along the line Y = X, suggesting that predicted pIC_{50} values were in good agreement with the actual pIC_{50} values and the 3D-QSAR models were of satisfactory predictive capability.

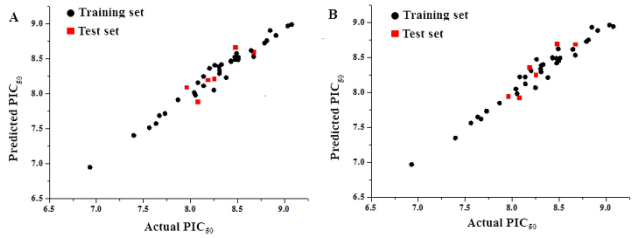

Figure 3. Plots of actual *versus* predicted pIC50 values for all the molecules based on CoMFA (A) and CoMSIA (B) models

2.2 CoMFA and CoMSIA contour maps

To visualize the field effects in 3D space, the information which provides by CoMFA and CoMSIA contour maps, offers theoretical support for designing novel and potent compounds. For the convenience of the analysis, the compound 26 (dabigatran) was employed to illustrate the key structural features. The default values of the favorable and unfavorable contours represented 80% and 20% level contribution.

The Figure 4A was the contour map of the steric field in CoMFA model. The green contours indicated that the bulky groups are conducive to activity, whereas yellow ones meant the bulky groups can result in the decreased activity. On the pyridine ring, there was a medium-sized green contour, which indicates that the large group is beneficial to the improvement of activity. In the electrostatic contour map of the CoMFA model, the electrostatic favorable and unfavorable regions were represented by blue and red contours, respectively. In Figure 4B, it can be found that the 3-, 4- and 5- position in the A location were surrounded by a large blue contour, indicating that the positive electricity group is advantageous for the improvement of activity.

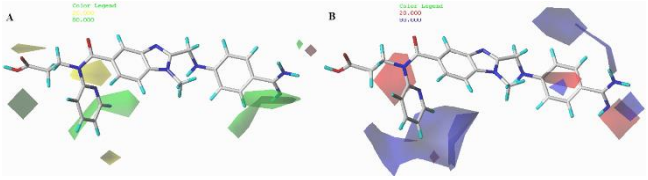

Figure 4. Steric and electrostatic contour maps of the CoMFA model

The steric and electrostatic contour maps of CoMSIA model were shown in Figure

5AB. Not surprisingly, the information of contour maps were basically similar to those of CoMFA model, hence they were not discussed. In the hydrophobic field of CoMSIA model (Figure 5C), hydrophobic favorable and unfavorable areas were exhibited by yellow and white contours, respectively. The A position was surrounded by a large yellow contours, which indicates the hydrophobic property in this place may increase its activity. The H-bond donor/acceptor fields of the CoMSIA model were described in Figure 5D and Figure 5E. The favorable and unfavorable regions in H-bond donor field were represented by cyan and purple contours, and in the H-bond acceptor field, they were revealed by magenta and red contours. As shown in Figure 5D and 5E, the red contours of the H-bond acceptor field almost coincide with the cyan contours of the H-bond donor field, which indicated the consistency of the established models.

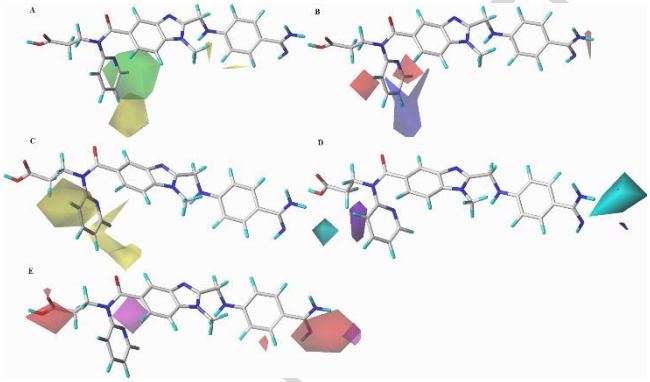

Figure 5. Steric (A), electrostatic (B), hydrophobic (C), H-bond acceptor (D) and H-bond donor (E) contour maps of the CoMSIA model.

2.3 Design of new dabigatran derivatives

According to the contour maps of CoMFA/CoMSIA models, some meaningful information about dabigatran derivatives as thrombin inhibitors was obtained, as shown in Figure 6. In general, the site of the compound was affected by several fields rather than a single field, so the field effects should be taken into account when designing the compound. Dabigatran was taken as a template to design new inhibitors. Combining with the structure-activity relationship in Figure 6, increased electron density on aromatic rings is beneficial to activity, hence the benzene ring replaces the pyridine ring to increase the electron density. At the A position, the large and hydrophobic groups favor activity. Then the -Cl group was designed at the 2-, 3-, and 4- position on the benzene ring. In the N-1 of benzimidazole at the B position, large but not huge and hydrophobic groups are beneficial for activity. In addition, the research(Li et al., 2015) also reported that ethyl group at N-1 of benzimidazole exhibites better anticoagulant activity against thrombin. Hence, the ethyl group with appropriate size and hydrophobicity was introduced. On the benzene ring at the C position, the F group was

Table 2 The predicted pIC50 values of the newly designed compounds

No.	Structure	PIC_{50}	
		Pred[a]	Pred[b]
Ref[c]	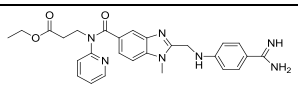	8.837	8.887
12a	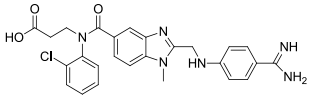	8.298	8.351
12b	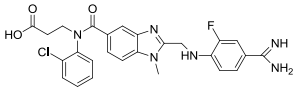	8.240	8.251
12c	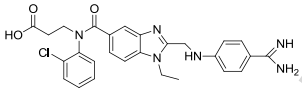	8.338	8.424
12d	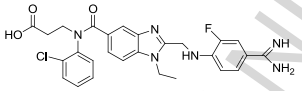	8.178	8.214
12e	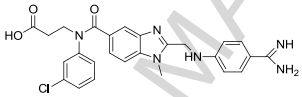	8.203	8.355
12f	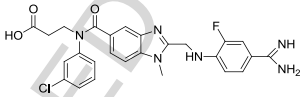	8.405	8.324
12g	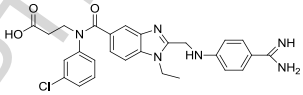	8.340	8.256
12h	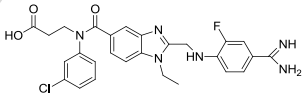	8.222	8.252
12i	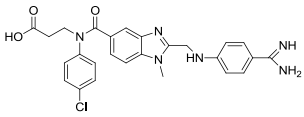	8.168	8.200
12j	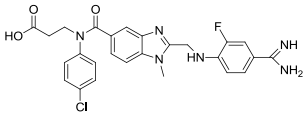	8.196	8.196
12k	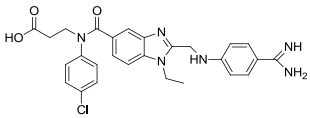	8.127	8.057

Pred[a]: predicted by CoMFA model

Pred[b]: predicted by CoMSIA model

Ref[c]: reference compound, dabigatran

introduced. With the introduction of fluorine group, the physical and chemical properties of drug molecules could be changed, which, in turn, alters the pharmacokinetic properties of drug molecules. Finally, 11 novel dabigatran derivatives (12a-12k) were designed and synthesized. The structures and the predicted pIC_{50} values of 12a-12k based on CoMFA and CoMSIA models were listed in Table 2. Table 2 shows that the pIC_{50} values of all designed new molecules within an order of magnitude, were comparable to dabigatran. It is suggested that they have good potential inhibitory activity, and further synthesis and bioactivity studies could be conducted.

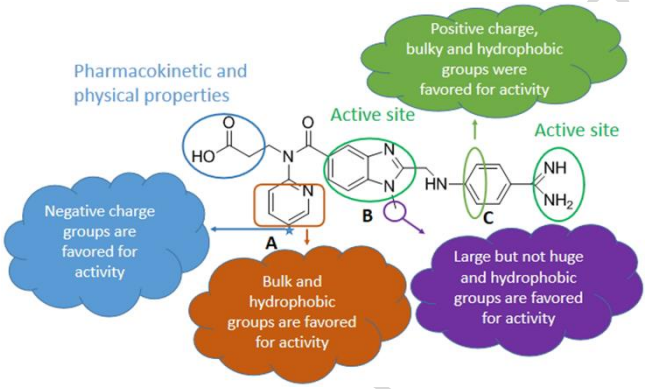

Figure 6. Structure–activity relationships derived from 3D-QSAR studies.

2.4 Molecular docking

Molecular docking explores the binding affinities of ligand and receptor, which helps us to further understand the quantitative structure-activity relationship. Before molecular docking, dabigatran was redocked to validate the docking reliability. As shown in Figure 7, the re-docking results showed that the conformations of dabigatran and the original ligand (red) almost overlapped in the active site (PDB code: 1KTS, resolution: 2.4 Å). The aromatic ring of A position was positioned in the D-pocket which were similar to the results in literature(Hauel et al., 2002), indicating that the position in the receptor cavity was correct. Subsequently, the 11 designed compounds

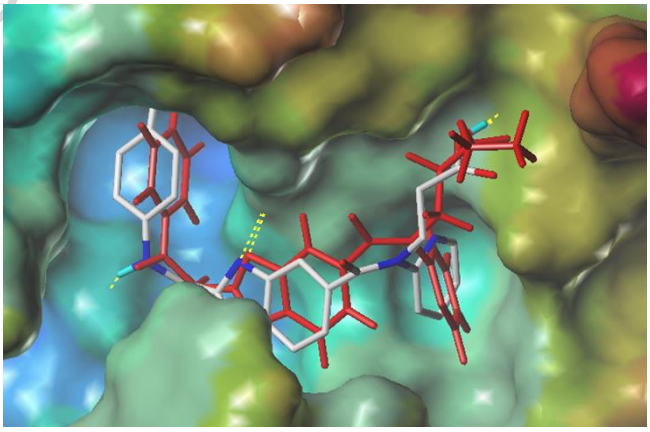

Figure 7. The re-docking result of dabigatran

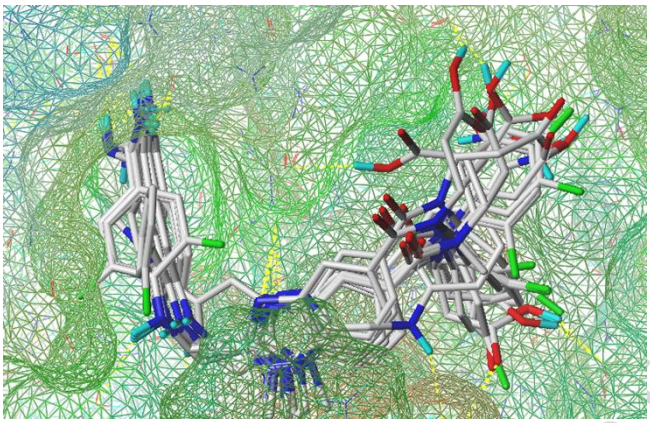

Figure 8. Docking results of all the compounds in thrombin protein (1KTS)

in this study were docked into thrombin receptor to analyze the bonding patterns. As shown in Figure 8, all the compounds maintained the similar U-shaped configurations and were buried deeply in the receptor cavity. H-bond interactions were found between the dabigatran derivatives and several key residues, such as Gly219, Asp189, Ala190 and Gly216. Figure 9A illustrates the interactions between dabigatran and surrounding residues in the active site. A total of six hydrogen bonds were formed. The observed hydrogen bond distances are 1.75 Å (Gly219-O···H-), 1.74 Å (Asp189-O···H-),

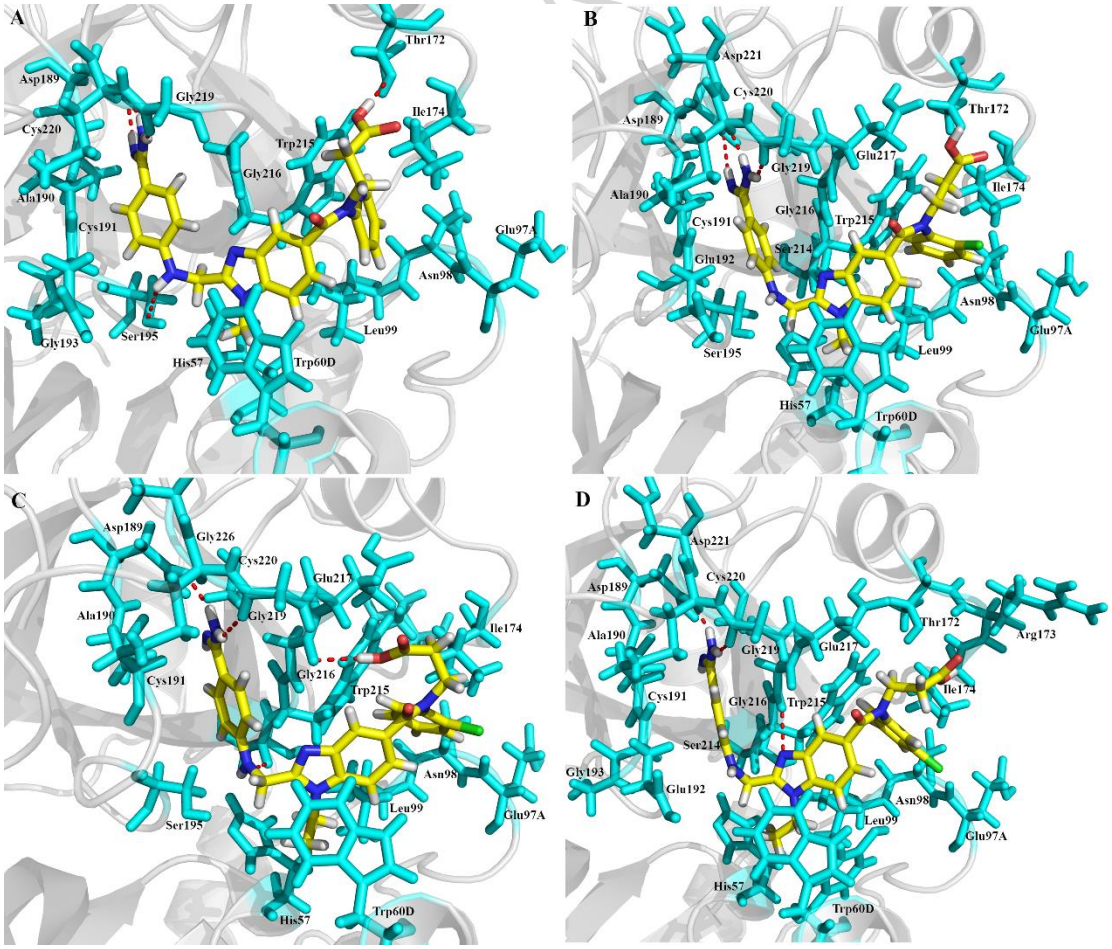

Figure 9. Docking result of compound dabigatran (A), 12a (B), 12c (C) and 12g (D).

2.17 Å (Asp189-O···H-), 2.42 Å (Asp189-O···H-), 2.75 Å (Ser195-O···H) and 2.08 Å (Thr172-O···H-), respectively. The amidine formed electrostatic interactions with amino acids Gly219, Asp189, Cys191, Ala190, Cys220, Asp221, Gly193. It was in agreement with the red contours of electrostatic field in the 3D-QSAR model. Pyridine rings produced van der Waals interaction with surrounding residues Asn98, Glue97A, Leu99, Trp215, which corresponds to the yellow contours of hydrophobic field. These results suggested that the molecular docking was agreement with the generated CoMFA/CoMSIA model.

In order to identify the more detailed interacting mode, three newly designed compounds (12a, 12c, and 12g) with better activity, were selected for an in-depth analysis. As showed in Figure 9B, a total of four hydrogen bonds were formed for 12a. The observed hydrogen bond distances are 1.89 Å (Gly219-O···H-), 2.09 Å (Asp189-O···H-), 2.45 Å (Asp189-O···H-) and 2.50 Å (Ala190-O···H-), respectively. Similarly, compounds 12c and 12g were docked into the same active site as shown in Figure 9C and 9D. A total of five hydrogen bonds were formed for 12c. The observed hydrogen bond distances are 2.33 Å (Gly219-O···H-), 2.02 Å (Asp189-O···H-), 2.25 Å (Asp189-N···H-), 2.47 Å (Ser214-O···H-) and 2.19 Å (Gly216-O···H-), respectively. For the

Table 3. Results of molecular docking for compounds 12a-12k

Com.	Total score	Crash	Polar	NHB[a]	Residues[b]
12a	8.4464	-2.1978	2.1626	4	Gly219, Asp189, Ala190
12b	9.766	-1.7153	3.2848	6	Gly219, Asp189, Ser195, Glu97A, Tyr60A
12c	9.5733	-2.9443	2.5557	5	Gly219, Asp189, Gly216, Ser214
12d	9.6787	-3.2373	3.3423	5	Gly219, Asp189, Glu217, Ser214
12e	8.1093	-2.5831	2.9361	3	Asp189, Tyr60A
12f	9.0084	-2.4020	3.0288	8	Gly219, Asp189, Ala190, Gly216, Glu97A
12g	7.8091	-2.1289	2.5458	3	Gly219, Asp189
12h	8.9843	-2.4749	2.2878	4	Gly219, Asp189, Gly216
12i	8.8057	-2.2709	3.0486	6	Gly219, Asp189, Gly216, Glu97A, Tyr60A
12j	8.0391	-1.6329	1.9081	4	Phe227, Trp215,Ser214, Pro60C
12k	7.9979	-3.0466	2.6556	5	Gly219, Asp189, Glu217, Ser214
Ref[c]	8.1128	-3.1800	2.1172	6	Gly219, Asp189, Ser195, Thr172

NHB[a]: Number of hydrogen bonds

Residues[b]: Residues and hydrogen bonding interaction

Ref[c]: reference compound, dabigatran

12g, there are three hydrogen bonds. The observed hydrogen bond distances are 2.00 Å (Gly219-O···H-), 1.89 Å (Asp189-O···H-) and 2.36 Å (Asp189-N···H-), respectively. By comparing the three docking compounds with the dabigatran, it is found that they all have hydrogen bonding with the common residues Gly219 and Asp189, and pi-pi interaction with the residue Trp60D. These results contribute to the identification of key residues that affect the activity and stability of ligands. At the same time, comparing the docking results of 12a, 12c, 12g and dabigatran, it can be found that they all maintain the similar U-shaped conformation with the receptor, but the C-ring positions of 12a, 12c and 12g have changed in conformation compared with the dabigatran, which makes them hard to interact with other key residues. The six number of hydrogen bonds were formed between the dabigatran and the receptor, which maintained its stability in the receptor. This may be the reason why their activity are slightly lower than the dabigatran. Figure 8 showed that the substituents of benzene ring are encapsulated by hydrophobic D-pockets, which shows that hydrophobic groups on benzene ring are crucial to the affinity of receptors and ligands. Meanwhile, it was found that the amidine formed stable hydrogen bonds with residues Gly219 and Asp189, and electrostatic interaction with residues Ala190, ASP189, Cys220, Asp221 and Ser195. The benzimidazole ring forms pi–pi stacking interactions with conserved Trp60D, and Van Der Waals interaction with residues Leu99, Tyr60A, Trp60D and Ser214. These interactions were very significant to improve the activity and stability of the inhibitor. Moreover, the binding interaction patterns were complementary to those of CoMFA and CoMSIA contour maps.

2.5 Analysis of MD simulation

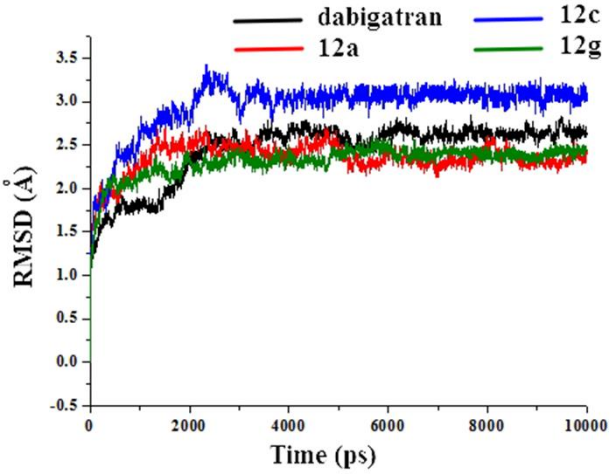

Figure 10. The root-mean-square deviation (RMSD) of dabigatran (black), 12a (red) 12c (blue) and 12g (green) in complexes obtained from 10 ns MD simulation.

In this study, the dynamics simulation of the dabigatran complex was initially carried out. The 10 ns MD simulations were performed on compounds dabigatran, 12a, 12c and 12g to further understand the detailed dynamic binding mode. The system overall convergence and stability of MD simulations were monitored by root-mean-square deviation (RMSD) of backbone atoms (C, Cα, N, and O) with respect to the initial docking structure. As show in Figure 10, the RMSD value of the four complexes was stable after 6 ns of simulation time. The fluctuations of dabigatran, 12a, 12c and 12g maintained at average 2.6 Å, 2.4 Å, 3.0 Å and 2.4 Å, suggesting the stability of the complex conformation. Thus, the subsequent MD simulations discussions would be reasonable to analyze the conformations that extracted from last 2 ns of MD trajectories. The superposition of the final structure of complex extracted from MD simulation (red) and the original docked structure (blue) was showed in Figure 11. The final simulation structure and the initial docked structure were in the same binding pocket from MD simulation (red) of dabigatran (A), 12a (B), 12 (C) and 12g (D), excepting for a slight drift. The H-bond distances of dabigatran (Figure 12A) were 2.39 Å (Gly219-O···H-), 2.91 Å (Asp189-O···H-) and 1.99 Å (Glu216-O···H-), respectively. After MD simulation, the conformation of dabigatran was extended in the pocket, which made it contact more residues and formed an additional H-bond with the residue Glu217. However, due to the extension of the conformation, the H-bond distance with the residues Asp189 and Gly219 becomes longer, which may increase the instability of the ligand in the receptor. The H-bond distances of 12a (Figure 12B) were 1.99 Å (Ser195-H···N-), 2.09 Å (Asp189-O···H-), 2.20 Å (Glu217-O···H-), 2.01 Å (Asn98-H···O-) and 1.90 Å (Arg93-O···H-), respectively. The H-bond distances of 12c (Figure 12C) was 2.35 Å (Asp189-O···H-). The H-bond distances of 12g (Figure 12D) were 2.42 Å (Gly219-H···N-), 1.89 Å (Glu217-O···H-), 2.70 Å (Asp186A-O···H-) and 2.37 Å (Trp60D-H···O-), respectively.

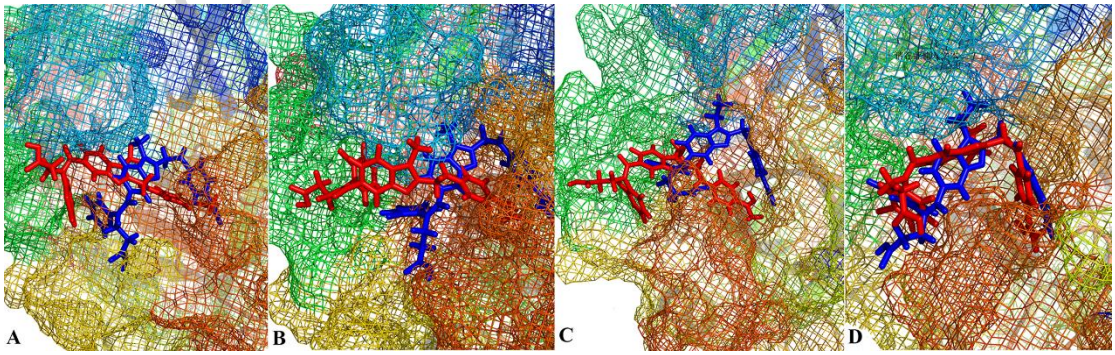

Figure 11. Structural comparison between initial (blue) and representative snapshots

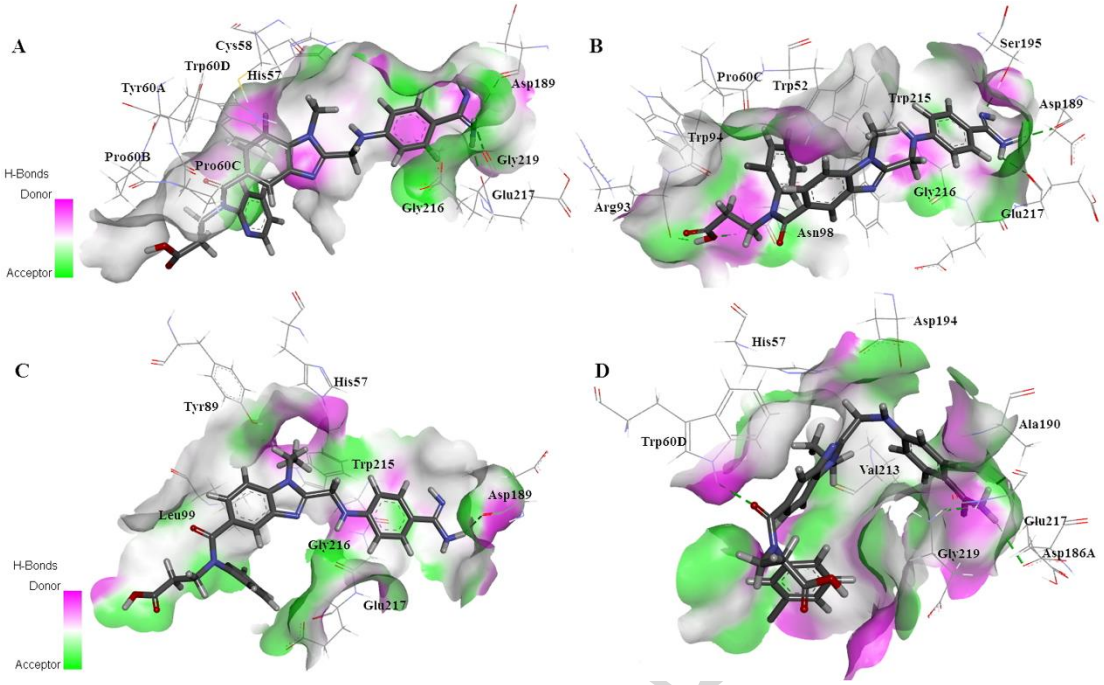

Figure 12. The binding mode of dabigatran (A), 12a (B), 12c (C) and 12g (D) after MD simulation.

Comparing the molecular dynamics results of 12a, 12c, 12g and dabigatran, it can be found that some distortions and changes occur in the spatial conformation after 10 ns of dynamics simulation. Dabigatran still maintains hydrogen bonding with key residues Gly219 and Asp189, while 12a, 12c and 12g have some extensions in space and cannot produce hydrogen bonding with key residues Gly219 and Asp189.

Based on the MD simulation, the binding free energy calculations for the four inhibitors of the last 2 ns trajectory were performed and are listed in Table 4. MM/PBSA and MM/GBSA were both used in free energy calculations. It can be seen from the Table 4 that van der Waals energy ΔE_{vdw} is the most important contribution to the overall binding energy, followed by electrostatic energy ΔE_{ele}. The binding free energies ΔG_{bind} of the inhibitors dabigatran, 12a, 12c and 12g *via* MM-GBSA were predicted to be -16.36, -23.94, -20.66, -19.66 kcal/mol, respectively, and *via* MM-PBSA were predicted to be -25.38, -28.24,-29.86 and -29.00 kcal/mol, respectively. From the two calculation methods of binding free energy ΔG_{bind}, it can be found that the ΔG_{bind} of the dabigatran complex was higher than that of 12a, 12c, and 12g, indicating that the stability of the three designed compound may be better than dabigatran. Although both MM/PBSA and MM/GBSA methods were adopted to calculate the binding free energy, in general, the MM/PBSA performs better than MM/GBSA in calculating binding free energy(Hou et al., 2011). In addition, the order of the binding energy of compounds 12c > 12g > 12a, was also consistent with the activity measured in our experiments. So,

the three designed compounds 12a, 12c and 12g could be used as good potential thrombin inhibitors.

Table 4. Average binding free energy (kcal mol^{-1}, last 2 ns) of complexes along with the different energy (kcal mol^{-1}, last 2 ns) contributions

NO.	ΔE_{vdw}	ΔE_{ele}	ΔG_{gas}	ΔG_{GB}	ΔG_{SA}	ΔG_{sol} (GB)	ΔG_{bind} (GB)	ΔG_{PB}	ΔG_{SA}	ΔG_{sol} (PB)	ΔG_{bind} (PB)
da	-47.37	-35.15	-82.52	71.20	-5.05	66.15	-16.36	63.10	-5.97	57.13	-25.38
12a	-45.02	-46.79	-91.81	72.36	-4.49	67.87	-23.94	69.29	-5.72	63.57	-28.24
12c	-46.99	-40.91	-87.90	72.12	-4.88	67.24	-20.66	62.19	-4.15	58.04	-29.86
12g	-46.67	-31.99	-78.65	63.92	-4.93	58.99	-19.66	55.25	-5.60	49.66	-29.00

2.6 ADME prediction

In the R&D process for new drugs, ADME and bioavailability analysis played significant roles in drug-likeness. The ADME parameters calculated by the SwissADME web tool for the designed compounds were summarized in Table 5. The results showed that the log P values of the synthesized compounds and dabigatran were in the range of -0.7 and 5.0, and the log S values were less than or equal to 6, indicating that they have the reasonable absorbency and good solubility in the body. With the introduction of the F group in the C ring, the water solubility predicted by ADME will increase. This is because F group has high electronegativity, and its attachment to benzene ring will increase electron cloud of benzene ring and polarization of adjacent NH bond, so the corresponding water solubility will increase.

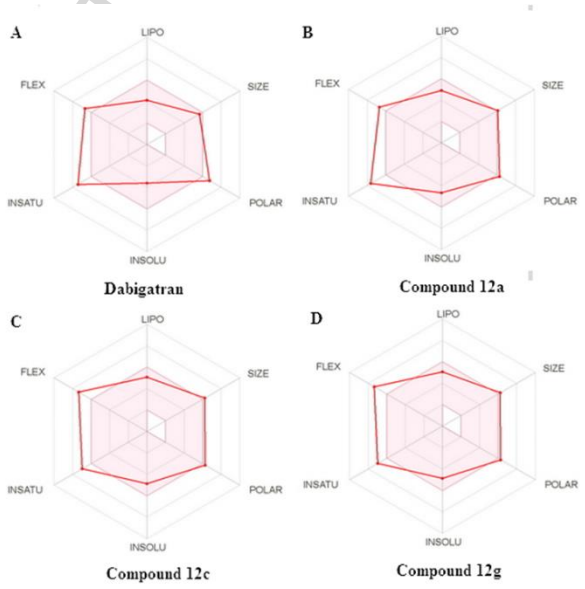

Figure 13. The bioavailability radars for dabigatran (A), 12a (B), 12c (c) and 12g (d).

Ligand lipophilicity efficiency (LLE) is the single parameter which considers the activity and lipophilicity of the compounds. It can be observed from Table 5 that the LLE values of most compounds were within the ideal range, except for compounds (12h and 12k) with LLE values of less than 5. Among the synthesized compounds, 12a had highest LLE value, indicating that it has potential beneficial activity in vivo.

The HIA and BBB values show that they had low intestinal absorption and no brain penetration. Compared with dabigatran, the eleven synthetic compounds have the inhibitory effect on cytochrome CYP1A2. It indicates that these compounds could prolong the action time of the drug, increase the blood concentration, and enhance the therapeutic effect of the drug by inhibiting cytochrome CYP1A2. At the same time, the incidence of side effects may also increase. Moreover, their Log Kp values were higher than that of dabigatran, indicating that the synthesized compounds have better permeability to the skin. Good skin permeability suggests that the compounds could easily penetrate the skin tissue when it is made into the external preparation. At the same time, they conformed to the Lipinski rules of druglikeness. The three highest bioactivity compounds (12c, 12a and 12g) and the reference dabigatran were further analyzed. The bioavailability radars of the four inhibitors were analyzed intuitively in Figure 13. The pink areas meant the optimum range of six properties, namely, lipophilicity, size, polarity, insolubility, instauration and flexibility. It can be seen from the Figure 13 that compounds 12c, 12a and 12g were almost within the range of conformity, except for the inconsistency of instauration and flexibility. Compared with dabigatran, the three designed compounds performed better in polarity. In short, the pharmacokinetic properties of eleven designed compounds are acceptable, and compounds 12a, 12c, and 12g have further research significance.

Table 5. ADME prediction of newly synthesized compounds

No.	Log P	TPSA (Å^2)	Log S	Fraction Csp^3	Rotatable bonds	LLE	HIA	BBB	CYP1A2 inhibition	Log Kp	Lipinski filter
12a	3.02	137.33	-4.67	0.15	10	6.081	Low	No	Yes	-7.21	Yes
12b	3.33	137.33	-4.83	0.15	10	5.559	Low	No	Yes	-7.25	Yes
12c	3.45	137.33	-4.87	0.19	11	5.561	Low	No	Yes	-7.08	Yes
12d	3.61	137.33	-5.03	0.19	11	5.058	Low	No	Yes	-7.12	Yes
12e	3.07	137.33	-4.67	0.15	10	5.657	Low	No	Yes	-7.21	Yes
12f	3.42	137.33	-4.83	0.15	10	5.193	Low	No	Yes	-7.25	Yes
12g	3.36	137.33	-4.87	0.19	11	5.140	Low	No	Yes	-7.08	Yes
12h	3.67	137.33	-5.03	0.19	11	4.667	Low	No	Yes	-7.12	Yes

12i	3.02	137.33	-4.67	0.15	10	5.231	Low	No	Yes	-7.21	Yes
12j	3.32	137.33	-4.83	0.15	10	5.234	Low	No	Yes	-7.25	Yes
12k	3.36	137.33	-4.87	0.19	11	4.986	Low	No	Yes	-7.08	Yes
dabigatran	1.94	150.22	-3.62	0.16	10	7.940	Low	No	No	-7.97	Yes

2.7 Chemistry

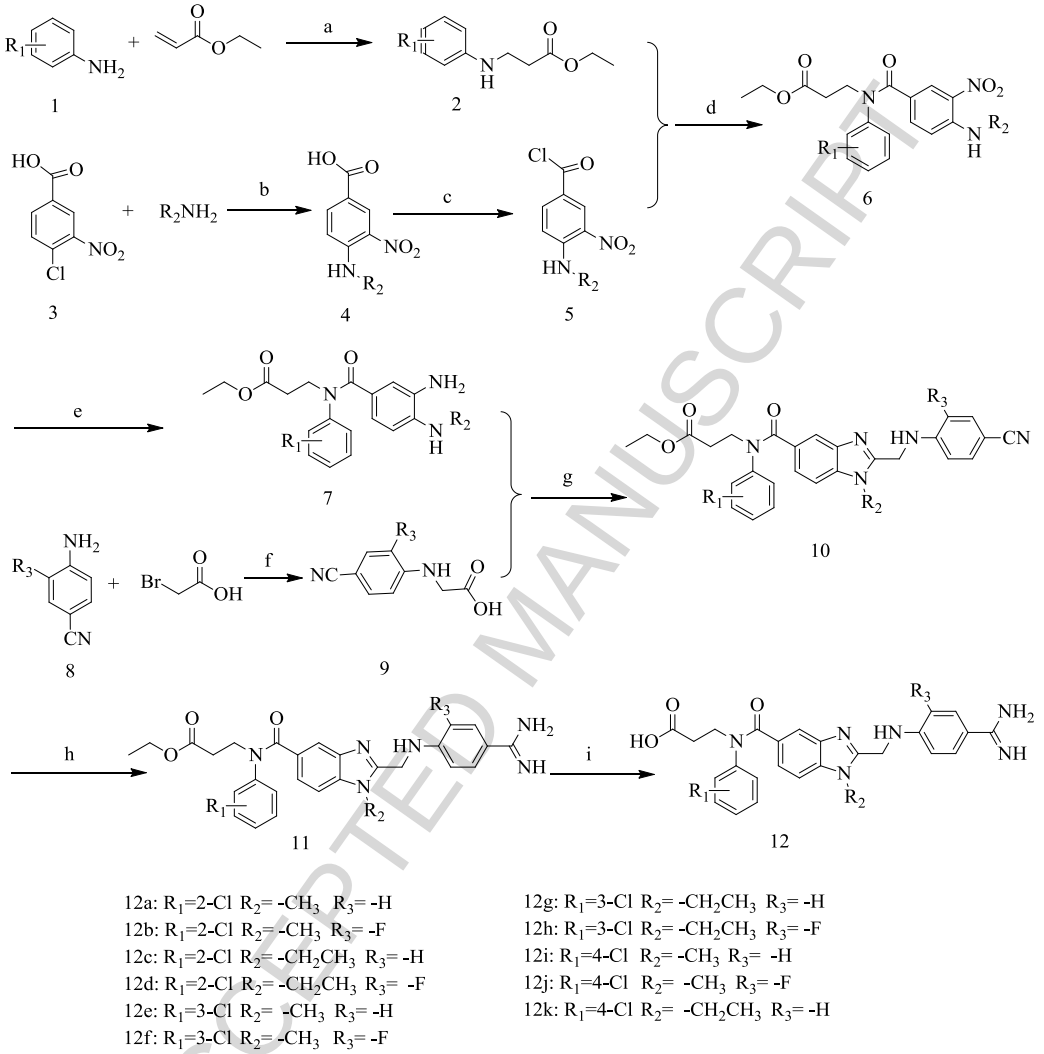

Scheme 1. Synthesis of compounds 12a-k. Reagents and conditions: (a) TfOH (10 mol%), 12 h, 100°C, yields: 38-82%; (b) amine, 80°C, 5 h; AcOH, pH 4–5, yields: 90%-95%; (c) DCM, $SOCl_2$, rt, 2 h, yields: 100%; (d) DCM, Et_3N, rt, 3 h, yields: 24-76%; (e) Zn, AcOH, THF/H_2O, rt, yields: 59-78%; (f) H_2O, 100°C; (g) EDCI, HOBt, DMF/THF; AcOH, ammonium hydroxide, yields: 45–82%; (h) $NH_2OH{\cdot}HCl$, Et_3N, anhydrous ethanol; Pd/C, $HCOONH_4$, AcOH, N_2, yields: 50-79%; (i) NaOH, H_2O/EtOH, rt, 2 h, yields: 72-87%.

The reaction route of dabigatran derivatives was presented in the Scheme 1. First, intermediate compounds (2a-2k) were prepared from aniline (1) and ethyl acrylate with trifluoromethanesulfonic acid (TfOH) (10% mol) as a catalyst. The reaction mixtures was heated and refluxed for 12 h under N_2 atmosphere. Reaction of 4-chloro-3-

nitrobenzoic acid (3) and the readily available amine solution yielded 4-substituted-3-nitrobenzoic acids (4a-4k) in good yield. Compounds 4a-4k were converted to 5a-5g by chlorination. Acylation of compound 2a-k with chlorides 5a-5k under alkaline conditions gave 6a-6k. Reaction of the nitro compounds 6a-6k with the reducing agent Zn/AcOH furnished amino compounds 7a-7k. Compounds 8 and bromoacetic acid were mixed and stirred at 100℃ to obtain compound 9. 7a-7k were reacted with compounds 9 in the presence of 1-(3-dimethylaminopropyl)-3-ethylcarbodiimide hydrochloride (EDCI) and 1-hydroxybenzotriazole (HOBt) to afford the imidazole compounds 10a-10k. 10a-10k were reacted with hydroxylamine hydrochloride in triethylamine (TEA) to obtain compounds 11a-11k. The target compounds 12a-12k were obtained from 11a-11k via hydrolysis. The structures of the synthesized compounds were determined from their ^{1}H NMR, ^{13}C NMR and HR-MS data before the biological evaluation.

2.8 Anticoagulant activity in vitro

The inhibitory activity of compounds 12a-12k against thrombin were evaluated by chromogenic assays. Argatroban and dabigatran were used as positive control. The IC_{50} values of compounds 12a-12k were evaluated and the corresponding data were listed in Table 6. The results of activity test showed that the inhibitory rate of all compounds were above 95%, which indicated that the designed compounds had good inhibitory

Table 6. Thrombin inhibitory activity (IC_{50}) of new dabigatran derivatives.

NO.	compound	IC_{50}(nM)	pIC_{50}	Inhibition rate(%)
1	12a	11.19±1.70	7.951	96.58
2	12b	14.16±1.87	7.849	97.67
3	12c	10.94±1.85	7.961	99.70
4	12d	13.25±3.78	7.878	100.00
5	12e	11.84±1.33	7.927	97.59
6	12f	13.10±1.69	7.883	97.05
7	12g	11.49±2.57	7.940	100.00
8	12h	12.96±1.30	7.887	96.96
9	12i	31.55±4.81	7.501	96.75
10	12j	11.91±1.38	7.924	97.72
11	12k	16.36±1.70	7.786	96.97
12	Dabigatran	9.99±1.48	8.000	99.10
13	Argatroban	7.61±0.81	8.119	-

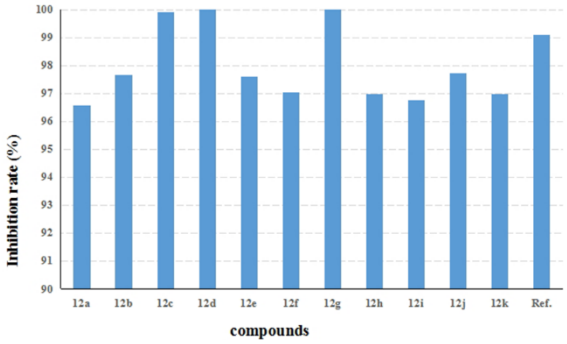

Figure 14. The thrombin inhibition rate of compound 12a-12k (Ref[c]: reference compound, dabigatran).

activity. The results also showed that the designed compounds exhibited moderate to good thrombin inhibitory activity compared to dabigatran. Especially, compounds 12a-12h, 12j and 12k showed similar equivalent inhibitory activity to the references, with IC_{50} values of 11.19 ±1.70 nM, 14.16 ± 1.87 nM, 10.94 ± 1.85 nM, 13.25 ± 3.78 nM, 11.84 ± 1.33 nM, 13.10 ± 1.69 nM, 11.49 ± 2.57 nM, 12.96 ± 1.30 nM, 11.91 ± 1.38 nM and 16.36 ± 1.70 nM, respectively. Furthermore, compound 12c was found to be the most potent thrombin inhibitor among all these new compounds, which was comparable to dabigatran (IC_{50} value: 9.99 ± 1.48 nM). Comparing the predicted pIC_{50} values and measured values of the synthesized compounds, it could be found that the measured pIC_{50} values are comparable to or not much different from dabigatran, which is similar to the predicted results. Moreover, the measured values of 12a, 12C and 12g were higher, while the 12i and 12k were lower, which was consistent with the predicted results. These findings validated the reliability and predictive ability of our QSAR models.

The positions of the substituent groups exerted some impact on activity. It can be observed from the bioactivity results that the -Cl groups at the 2- position of the A location have higher bioactivity than 3- and 4-position. And when the -Cl group is at the 4-position, the -F group introduced at the C location will increase its bioactivity. Moreover, when the -Cl group is at the 2- and 3-position of the A location, the ethyl group introduced at benzimidazole ring will raise its bioactivity than that of methyl group. Compounds with ortho-substituents on benzene rings have anticoagulant activity. From the perspective of contour maps, the adjacent substituent -Cl on benzene ring corresponded to the green contour in the steric field of CoMFA/CoMSIA model. Ethyl substitution at N-1 of benzimidazole, which can fill the active pocket and have hydrophobic interactions with the surrounding residues, exhibited improved anticoagulant activity. The good activity of substituted ethyl on benzimidazole was also

consistent with the result discussed by our previous research group(Li et al., 2015), that is, ethyl substituents were beneficial to the improvement of inhibitor activity. From the molecular docking point of view, compound 12c produced two additional hydrogen bonds with the thrombin receptor, the N atom of benzimidazole formed one hydrogen bonding interaction with the residue Ser214 at distance of 2.47 Å, and hydrogen atom at carboxyl was hydrogen bonded to the residue Gly216 at distance of 2.19 Å. These effects have an impact on the improvement in the activity and stability of the inhibitor.

3. Conclusion

In this study, 42 dabigatran derivatives reported by our group as thrombin inhibitors were analyzed using computer-aided drug design methods, including 3D-QSAR, molecular docking and MD simulations. 3D-QSAR models with high reliability and predictive abilities were developed to discover the key structural factors that influence the anticoagulant activities. Reliable CoMFA (q^2 = 0.705, r^2 = 0.971) and CoMSIA (q^2 = 0.707, r^2 = 0.966) models were established and assisted with the internal and external validation. Molecular docking and MD simulations indicated that strong hydrogen bond and pi–pi stacking interactions with key residues Gly219, Asp189 and Trp60D played a key role in ligand binding with the receptor. Results showed that the 3D-QSAR, molecular docking and MD simulations were consistent with each other. Based on the above results, 11 novel candidate compounds (12a-12k) were designed and synthesized. The structures of the compounds were characterized by ^{1}H NMR, ^{13}C NMR and HR-MS. The results of the anticoagulant activity showed that the bioactivity of all the designed compounds were comparable to that of the reference dabigatran (IC_{50} = 9.99±1.48 nM). The order is 12c > 12a > 12g > 12e > 12j > 12h > 12f > 12d > 12b > 12k > 12i. The -Cl groups in the A location have higher bioactivity than 3- and 4-position, and when the -Cl group is at the 4-position, the -F group introduced at the C location will obviously increase its bioactivity. Moreover, when the -Cl group is at the 2- and 3-position of the A location, the ethyl group introduced at benzimidazole ring will raise its bioactivity than that of methyl group. Compounds with ortho-substituents on benzene rings have anticoagulant activity. In particular, 12a, 12c and 12g showed better anticoagulant activities with IC_{50} values of 11.19 ± 1.70, 10.94 ± 1.85 and 11.49 ± 2.57 nM, respectively, which were equivalent to the dabigatran. Compounds 12a, 12c and 12g are candidates for further exploration of potential novel anticoagulant drugs.

4. Experimental section

4.1 Chemistry

All chemicals and solvents were purchased from Darui and Titan Corporation and

used without further purification. Melting points were determined on WRS-1B and were uncorrected. NMR spectra were recorded on a Bruker Avance 500 MHz NMR spectrometer using TMS as internal reference. Chemical shifts are reported in δ scale (ppm). Mass spectra were acquired on a Solari X-70FT-MS apparatus. Thin-layer chromatography (TLC) was performed on silica gel plates (GF254) with visualization of components by UV light (254 nm). Column chromatography was carried out on silica gel (200–300 mesh). A series of novel dabigatran analogues were synthesized by the method described in Scheme 1)

4.1.1 3-(2-(((4-carbamimidoylphenyl)amino)methyl)-N-(2-chlorophenyl)-1-methyl-1H-benzo[d]imidazole-5-carboxamido)propanoic acid(12a)

White solid; yield; 72.4%; mp: 223.1-224.3℃; ^{1}H NMR (500 MHz, DMSO-d_6+^{2}HCl) δ (ppm) 9.09 (s, 1H), 8.78 (s, 1H), 7.72 (d, *J*=7.2 Hz, 2H), 7.56 (d, *J*= 7.6 Hz, 2H), 7.51 (m, 1H), 7.34 (d, *J* = 7.5 Hz, 2H), 7.22 (d, *J* = 7.2 Hz, 2H), 6.89 (s, 2H), 4.80 (s, 2H), 4.19 (t, *J*=7.2 Hz, 2H), 3.84 (s, 3H), 2.62 (t, *J* = 7.4 Hz, 2H); 13C NMR (125 MHz, DMSO-d_6) δ (ppm) 172.98, 170.12, 164.72, 153.90, 153.09, 140.33, 136.68, 136.65, 135.81, 131.98, 131.68, 130.71, 130.20, 128.82, 124.28, 122.96, 116.91, 114.31, 112.48, 111.13, 45.79, 32.43, 31.25, 29.79; HR-MS: calcd for $C_{26}H_{25}ClN_6O_3$ $(M+H)^+$, 505.17494, found 505.17415.

4.1.2 3-(2-(((4-carbamimidoyl-2-fluorophenyl)amino)methyl)-N-(2-chlorophenyl)-1-methyl-1H-benzo[d]imidazole-5-carboxamido)propanoic acid (12b)

White solid; Yield: 87.2%; m.p. 239.8-241.2℃;^{1}H NMR (500 MHz, DMSO-d_6+^{2}HCl) δ (ppm) 9.08 (s, 1H), 8.79 (s, 1H), 7.73 (t, *J* = 11.5 Hz, 2H), 7.63-7.50 (m, 2H), 7.40 (d, *J* = 9.4 Hz, 3H), 7.28 (d, *J* = 7.8 Hz, 1H), 7.24 (d, *J* = 8.0 Hz, 1H), 7.02 (t, *J* = 8.7 Hz, 1H), 4.92 (s, 2H), 4.05 (t, J= 7.2Hz, 2H), 3.89 (s, 3H), 2.61 (t, *J* = 7.8 Hz, 2H); ^{13}C NMR (125 MHz, DMSO-d_6+^{2}HCl) δ (ppm) 173.03, 172.99, 169.76, 164.12, 153.34, 151.15, 149.24, 141.51, 141.42, 143.31 ,139.24 , 135.60, 129.38, 128.61, 128.03, 126.46, 125.81, 124.69, 114.89, 114.41, 112.16, 111.07, 46.83, 32.64, 31.14, 21.27; HR-MS: calcd for $C_{26}H_{24}ClFN_6O_3$ $(M+H)^+$, 523.16552, found 523.16408.

4.1.3 3-(2-(((4-carbamimidoylphenyl)amino)methyl)-N-(2-chlorophenyl)-1-ethyl-1H-benzo[d]imidazole-5-carboxamido)propanoic acid (12c)

White solid; Yield: 74.5%; m.p. 266.4-267.2℃; ^{1}H NMR (500 MHz, DMSO-d_6+^{2}HCl) δ (ppm) 9.08 (s, 1H), 8.87 (s, 1H), 7.73 (d, *J* = 8.5 Hz, 2H), 7.68 (d, *J* = 10.1 Hz, 2H), 7.57 (d, *J* = 7.7 Hz 1H), 7.45-7.39 (m, 1H), 7.29 (t, *J* = 7.9 Hz , 1H), 7.24 (s, 2H), 6.91(d, *J* = 8.5Hz,2H), 5.01 (s, 2H), 4.48 (m, 2H), 4.20(t, *J*= 7.2 Hz, 2H), 2.60 (t, *J* = 7.4 Hz, 2H), 1.33 (t, *J* = 7.2Hz, 3H); ^{13}C NMR (125 MHz, DMSO-d_6+^{2}HCl) δ (ppm) 172.93, 169.92, 164.70, 164.88, 156.00, 153.28, 152.92, 150.00, 148.65, 134.54, 132.81, 130.24, 125.01, 123.30, 122.57, 117.05, 114.52, 113.37, 112.44, 111.75, 56.43, 45.26, 33.03, 20.83, 18.91; HR-MS: calcd for $C_{27}H_{27}ClN_6O_3$ $(M+H)^+$, 519.19059, found

519.19428.

4.1.4 3-(2-(((4-carbamimidoyl-2-fluorophenyl)amino)methyl)-N-(2-chlorophenyl)-1-ethyl-1H-benzo[d]imidazole-5-carboxamido)propanoic acid (12d)

White solid; Yield: 77.0%; m.p. 232.3-234.1℃; ^{1}H NMR (500 MHz, DMSO-d_6+^{2}HCl) δ (ppm) 9.43 (s, 1H), 9.21 (s, 1H), 7.96 (s, 1H), 7.90 (d, *J* = 8.6 Hz, 1H), 7.80 (d, *J* = 14.3 Hz, 1H), 7.67 (s, 1H), 7.58 (d, *J* = 7.6 Hz 1H), 7.50 (d, *J* = 8.5Hz, 1H), 7.42 (d, *J* = 7.7 Hz , 1H), 7.30 (t, *J* = 6.1Hz,1H), 7.26(d, *J* = 8.1Hz, 1H), 7.09(s, 1H), 5.01 (s, 2H), 4.45(m, 2H), 4.09 (t, *J* = 7.4Hz, 2H), 2.61 (t, *J* = 7.4 Hz, 2H), 1.33 (t, *J* = 7.2Hz, 3H); ^{13}C NMR (125 MHz, DMSO-d_6+^{2}HCl) δ(ppm) 173.09, 171.02, 164.75, 162.45, 160.11, 160.00, 153.44, 153,18, 141.16, 136.37, 132.04, 130.15, 129.33, 122.88, 119.36, 112.84, 112.62, 112.15, 110.09, 105.43, 105.17, 104.92, 46.29, 38.88, 32.78, 21.52, 15.28; HR-MS: calcd for $C_{27}H_{26}ClFN_6O_3$ $(M+H)^+$, 537.18117, found 537.18009.

4.1.5 3-(2-(((4-carbamimidoylphenyl)amino)methyl)-N-(3-chlorophenyl)-1-methyl-1H-benzo[d]imidazole-5-carboxamido)propanoic acid (12e)

White solid; Yield: 85.3%; m.p. 277.5-279.3℃; ^{1}H NMR (500 MHz, DMSO-d_6+^{2}HCl) δ 9.05 (s, 1H), 8.82 (s, 1H), 7.73 (t, *J* = 8.2 Hz, 3H), 7.64 (s, 1H), 7.40 (d, *J* = 8.7 Hz, 1H), 7.24 (d, *J* = 7.3 Hz, 3H), 7.15 (d, *J* = 6.9 Hz, 1H), 6.91 (d, *J* = 8.5 Hz, 2H), 4.94 (s, 2H), 4.06 (t, *J* = 7.4 Hz, 2H), 3.80 (s, 3H), 2.55 (t, *J* = 7.5 Hz, 2H); ^{13}C NMR (125 MHz, DMSO-d_6+^{2}HCl) δ 173.00, 169.97, 169.75, 164.15, 153.29, 151.15, 149.24, 141.51, 140.88, 136.49, 136.41, 130.21, 128.27, 128.24, 126.45, 124.75, 114.89, 114.72, 112.14, 111.04, 46.76, 32.64, 31.13, 20.91; HR-MS: calcd for $C_{26}H_{25}ClN_6O_3$ $(M+H)^+$, 505.17494, found 505.17103.

4.1.6 3-(2-(((4-carbamimidoyl-2-fluorophenyl)amino)methyl)-N-(3-chlorophenyl)-1-methyl-1H-benzo[d]imidazole-5-carboxamido)propanoic acid (12f)

White solid; Yield: 76.3%; m.p. 274.9-275.6℃; ^{1}H NMR (500 MHz, DMSO-d_6+^{2}HCl) δ (ppm) 9.25 (s, 1H), 8.95 (s, 1H), 7.78 (d, *J* = 7.2 Hz, 1H), 7.63 (s, 1H), 7.56 (s, 2H), 7.28 (m, 1H), 7.25 (d, *J* = 8.5 Hz, 4H), 7.12 (m, 1H), 7.04 (s, 1H), 4.88 (s, 2H), 4.04 (t, *J*=7.2 Hz, 2H), 3.85 (s, 3H), 2.54 (s, 2H); ^{13}C NMR (125 MHz, DMSO-d_6+^{2}HCl) δ (ppm) 173.01, 169.89, 166.02, 164.02, 155.43, 151.13, 149.21, 143.32, 141.45, 135.64, 132.17, 129.74, 128.44, 127.36, 126.52, 124.72, 117.52, 114.91, 114.74, 113.92, 112.11, 111.11, 46.77, 32.62, 31.22, 26.87; HR-MS: calcd for $C_{26}H_{24}ClFN_6O_3$ $(M+H)^+$, 521.16244, found 521.16284.

4.1.7 3-(2-(((4-carbamimidoylphenyl)amino)methyl)-N-(3-chlorophenyl)-1-ethyl-1H-benzo[d]imidazole-5-carboxamido)propanoic acid (12g)

White solid; Yield: 76.5%; m.p. 267.1-267.9℃; ^{1}H NMR (500 MHz, DMSO-d_6+^{2}HCl) δ (ppm) 9.03 (s, 1H), 8.81 (s, 1H), 7.71 (d, *J*=8.5 Hz, 2H), 7.72 (d, *J* = 8.8 Hz, 2H), 7.51 (s, 1H), 7.45 (d, *J* = 8.6 Hz, 1H), 7.24 (s, 2H), 7.17 (d, *J* = 6.4 Hz, 1H), 6.91 (d, *J* =8.3 Hz, 2H), 4.98 (s, 2H), 4.47 (m, 2H), 4.04 (t, *J* = 7.4 Hz, 2H), 2.56 (t, *J* = 7.3 Hz, 2H), 1.34 (t, *J* = 7.1 Hz,3H); ^{13}C NMR (125 MHz,

DMSO-d_6+^{2}HCl) δ (ppm) 173.04, 170.58, 164,72, 154.03, 153.35, 153.22, 149.19, 139.03, 136.26, 131.26, 130.50, 130.33, 130.17, 123.64, 122.06, 119.57, 113.73, 113.30, 112.19, 110.36, 56.47, 45.00, 33.13, 18.87, 15.25; HR-MS: calcd for $C_{27}H_{27}ClN_6O_3$ $(M+H)^+$, 519.19059, found 519.19132.

4.1.8 3-(2-(((4-carbamimidoyl-2-fluorophenyl)amino)methyl)-N-(3-chlorophenyl)-1-ethyl-1H-benzo[d]imidazole-5-carboxamido)propanoic acid (12h)

White solid; Yield: 80.2%; m.p. 236.3-237.5℃; ^{1}H NMR (500 MHz, DMSO-d_6+^{2}HCl) δ (ppm) 9.26 (s, 1H), 9.03 (s, 1H), 7.83 (d, *J* = 13.5 Hz, 2H), 7.67 (d, *J* = 16.5 Hz, 2H), 7.50 (s, 1H), 7.45 (s, 1H), 7.15 (s, 1H), 7.07 (d, *J* = 8.6 Hz, 2H), 6.94 (dd, *J* = 21.0, 7.8 Hz, 2H), 5.06 (s, 2H), 4.49 (m, 2H), 4.02 (t, *J* = 7.5 Hz, 2H), 2.54 (t, *J* = 14.8 Hz, 2H), 1.33 (t, *J*=7.2 Hz, 3H); ^{13}C NMR (125 MHz, DMSO-d_6+^{2}HCl) δ (ppm) 173.02, 170.05, 167.96, 164.88, 160.46, 153.70, 153.31, 151.28, 143.66, 141.95, 136.22, 130.14, 129.67, 128.44, 127.16, 126.14, 124.65, 124.20, 114.18, 112.37, 110.80, 110.52, 52.04, 49.06, 46.79, 32.68, 30.83; HR-MS: calcd for $C_{27}H_{26}ClFN_6O_3$ $(M+H)^+$, 537.18117, found 537.18009.

4.1.9 3-(2-(((4-carbamimidoylphenyl)amino)methyl)-N-(4-chlorophenyl)-1-methyl-1H-benzo[d]imidazole-5-carboxamido)propanoic acid(12i)

White solid; Yield: 74.3%; m.p. 253.5-254.3℃; ^{1}H NMR (500 MHz, DMSO-d_6+^{2}HCl) δ (ppm) 9.08 (s, 1H), 8.77 (s, 1H), 7.72 (d, *J* = 7.2 Hz, 2H), 7.57 (d, *J* = 8.5 Hz, 2H), 7.26 (t, *J* = 7.2 Hz, 3H), 7.21 (m, 2H), 6.89 (s, 2H), 4.81 (s, 2H),4.04 (t, *J* = 7.4 Hz, 2H), 3.86 (s, 3H), 2.56 (t, *J* = 7.5 Hz, 2H); ^{13}C NMR (125 MHz, DMSO-d_6+^{2}HCl) δ (ppm) 172.86, 171.43, 168.80, 164.89, 153.89, 152.66, 146.55, 144.12, 141.57, 134.42, 133.83, 131.92, 130.44, 130.24, 129.74, 126.20, 121.07, 119.21, 115.03, 114.82, 112.78, 46.58, 32.54, 32.12, 20.24; HR-MS: calcd for $C_{26}H_{25}ClN_6O_3$ $(M+H)^+$, 505.17494, found 505.17854.

4.1.10 3-(2-(((4-carbamimidoyl-2-fluorophenyl)amino)methyl)-N-(4-chlorophenyl)-1-methyl-1H-benzo[d]imidazole-5-carboxamido)propanoic acid (12j)

White solid; Yield: 85.3%; m.p. 277.5-279.3℃; ^{1}H NMR (500 MHz, DMSO-d_6+^{2}HCl) δ (ppm) 9.16 (s, 1H), 8.82 (s, 1H), 7.65 (d, *J* = 7.2 Hz, 3H), 7.50 (m, 1H), 7.25 (d, *J*=7.4 Hz, 2H), 7.09 (d, *J* = 8.7 Hz, 2H), 6.98 (m, 1H), 6.87 (t, *J* = 7.2 Hz, 2H), 4.93 (s, 2H), 4.05 (t, *J* = 7.4 Hz, 2H), 3.85 (s, 2H), 2.54 (t, *J* = 7.5 Hz, 2H); ^{13}C NMR (125 MHz, DMSO-d_6+^{2}HCl) δ (ppm) 177.66, 173.64, 167.94, 163.02, 159.93, 158.11, 154.16, 149.17, 147.31, 145.59, 138.94, 138.44, 136.64, 135.17, 134.60, 133.29, 131.28, 119.51, 116.53, 50.94, 41.02, 37.23, 36.91; HR-MS: calcd for $C_{26}H_{24}ClFN_6O_3$ $(M+H)^+$, 523.16552, found 523,16514.

4.1.11 3-(2-(((4-carbamimidoylphenyl)amino)methyl)-N-(4-chlorophenyl)-1-ethyl-1H-benzo[d]imidazole-5-carboxamido)propanoic acid (12k)

White solid; Yield: 80.2%; m.p. 235.8-236.3℃; ^{1}H NMR (500 MHz, DMSO-d_6+^{2}HCl) δ (ppm) 9.33 (s, 1H), 9.06 (s, 1H), 7.84 (d, *J* = 7.2 Hz, 2H), 7.66 (d, *J*=7.2 Hz, 2H),7.43 (m, 1H), 7.29 (d, *J* = 8.5

Hz, 2H), 7.22 (s, 3H), 7.14 (s, 1H),7.06 (s, 1H), 5.17 (s, 2H), 5.08 (m, 2H),4.04 (t, *J*=7.2 Hz, 2H), 3.16 (s, 2H), 2.54 (t, *J* = 7.4 Hz, 2H), 1.32 (t, *J* = 7.2 Hz, 3H); ^{13}C NMR (125 MHz, DMSO-d_6+^{2}HCl) δ (ppm) 175.54, 172.89, 168.79, 164.26, 160.72, 153.01, 152.45, 150.13, 131.96, 130.39, 130.31, 129.85, 129.76, 128.54, 118.86, 114.57, 112.65, 106.31, 46.32, 41.07, 38.73, 32.49, 14.47; HR-MS: calcd for $C_{27}H_{27}ClN_6O_3$ $(M+H)^+$, 518.18277, found 518.18377.

4.2. Anticoagulant assay in vitro

The anticoagulant activities of the target compounds were tested in vitro with argatroban as reference.The lyophilized human thrombin (national standard) (5.4 μg/mL) , was purifed from human blood with the test compounds dissolved in DMSO in different dilutions added and pre-incubated for 10 min at 37 °C. Subsequently, Ac-FVR-AMC (5 μM), as a specifc fluorogenic thrombin substrate, was added to the system. Then Envision microplate reader (PerkinElmer) to detect the dynamic changes in relative fluorescence intensity for 10 min at room temperature. During the initial stage of the reaction, the slope of the linear enzyme dynamics curve was referred to as the initial velocity of enzyme reaction. Instrument settings: excitation wavelength, 355 nm; emission wavelength, 460 nm. Each well was measured 20 times every 20 s for 10 min. Then the change in fluorescence within a predetermined time was measured with these conditions. The reaction kinetic curve slope (V_{max}) was served as an activity indicator. The concentration was calculated with a 50 % inhibition of thrombin activity (IC_{50}) by following formulas:

Inhibition rate (%) = $[V_{DMSO}-V_{sample}]/V_{DMSO} \times 100\%$

V_{sample}: initial velocity of compound group; V_{DMSO}: initial velocity of blank group, treated with DMSO alone.

Inhibition rate (%) = $100/[1+10^{(Log\ IC50-X)h}]$

h: Hill coeffcient

Lyophilized human thrombin: The National Institute for the Control of Pharmaceutical and Biological Products,China.

Ac-FVR-AMC: Calbiochem.

All measurements were performed in duplicate; the mean values of both determinations are presented.

Acknowledgments

This work was support by Shanghai Natural Science Foundation (No.19ZR1455400).

Conflict of Interest

The authors declare no conflict of interest.

Reference

Ahmad, Y., Lip, G.Y.H., 2012. Dabigatran etexilate for the prevention of stroke and systemic embolism in atrial fibrillation: NICE guidance. Heart 98, 1404–1406. https://doi.org/10.1136/heartjnl-2012-302101

Amata, E., Marrazzo, A., Dichiara, M., Modica, M.N., Salerno, L., Prezzavento, O., Nastasi, G., Rescifina, A., Romeo, G., Pittalà, V., 2017. Heme Oxygenase Database (HemeOxDB) and QSAR Analysis of Isoform 1 Inhibitors. ChemMedChem 12, 1873–1881. https://doi.org/10.1002/cmdc.201700321

B., C.J.T., S., Z., K., C.C.K.N., A., L.D., 2007. The central role of thrombin in hemostasis. J. Thromb. Haemost. 5, 95–101. https://doi.org/10.1111/j.1538-7836.2007.02500.x

Berry, C.N., Girard, D., Lochot, S., Lecoffre, C., 1994. Antithrombotic actions of argatroban in rat models of venous, 'mixed' and arterial thrombosis, and its effects on the tail transection bleeding time. Br. J. Pharmacol. 113, 1209–1214. https://doi.org/10.1111/j.1476-5381.1994.tb17126.x

Blommel, M.L., Blommel, A.L., 2011. Dabigatran etexilate: A novel oral direct thrombin inhibitor. Am. J. Heal. Pharm. 68, 1506–1519. https://doi.org/10.2146/ajhp100348

Chaudhari, K., Hamad, B., Syed, B.A., 2014. Antithrombotic drugs market. Nat. Rev. Drug Discov. 13, 571–572.

Curto, A., Albaladejo, A., 2016. Implications of apixaban for dental treatments, Journal of Clinical and Experimental Dentistry, 8, e611–614. https://doi.org/10.4317/jced.53004

Dahl, O., 2008. Dabigatran etexilate: An oral direct thrombin inhibitor, Therapy, 5, 685–695. https://doi.org/10.2217/14750708.5.5.685

De Candia, E., 2012. Mechanisms of platelet activation by thrombin: A short history. Thromb. Res. 129, 250–256. https://doi.org/https://doi.org/10.1016/j.thromres.2011.11.001

Eriksson, B.I., Smith, H., Yasothan, U., Kirkpatrick, P., 2008. Dabigatran etexilate. Nat. Rev. Drug Discov. 7, 557–558.

Granger, C., H Alexander, J., Mcmurray, J., D Lopes, R., Hylek, E., Hanna, M., R Al-Khalidi, H., Ansell, J., Atar, D., Avezum, A., Cecilia, M., Bahit, R., Donald Diaz, J., A Easton, J., Ezekowitz, M., Ch, B., Flaker, G., Garcia, D., Geraldes, M., Wallentin, L., 2011. Apixaban versus Warfarin in Patients with Atrial Fibrillation. N Engl J Med. 365, 981–992. https://doi.org/10.1056/NEJMoa1107039)

Gustafsson, D., Antonsson, T., Bylund, R., Eriksson, U., Gyzander, E., Nilsson, I., Elg, M., Mattsson, C., Deinum, J., Pehrsson, S., Karlsson, O., Nilsson, A., Sörensen, H., 1998. Effects of melagatran, a new low-molecular-weight

thrombin inhibitor, on thrombin and fibrinolytic enzymes. Thromb. Haemost. 79, 110–118.

Haas, S., 2008. New oral Xa and IIa inhibitors: updates on clinical trial results. J. Thromb. Thrombolysis 25, 52–60. https://doi.org/10.1007/s11239-007-0108-7

Hauel, N.H., Nar, H., Priepke, H., Ries, U., Stassen, J.-M., Wienen, W., 2002. Structure-Based Design of Novel Potent Nonpeptide Thrombin Inhibitors. J. Med. Chem. 45, 1757–1766. https://doi.org/10.1021/jm0109513

Hou, T., Wang, J., Li, Y., Wang, W., 2011. Assessing the Performance of the MM/PBSA and MM/GBSA Methods. 1. The Accuracy of Binding Free Energy Calculations Based on Molecular Dynamics Simulations. J. Chem. Inf. Model. 51, 69–82. https://doi.org/10.1021/ci100275a

Huang, S., Feng, K., Ren, Y., 2019. Molecular modelling studies of quinazolinone derivatives as MMP-13 inhibitors by QSAR, molecular docking and molecular dynamics simulations techniques. Medchemcomm 10, 101–115. https://doi.org/10.1039/C8MD00375K

Kam, P.C.A., Kaur, N., Thong, C.L., 2005. Direct thrombin inhibitors: Pharmacology and clinical relevance. Anaesthesia 60, 565–574. https://doi.org/10.1111/j.1365-2044.2005.04192.x

Kim, S., Tran, N., Schewe, J., Boehm, O., Wittmann, M., Graeff, I., Hoeft, A., Baumgarten, G., 2015. Safety and economic considerations of argatroban use in critically ill patients : a retrospective analysis. Journal of Cardiothoracic Surgery, 10, 1–8. https://doi.org/10.1186/s13019-015-0214-0

Lee, C.J., Ansell, J.E., 2011. Direct thrombin inhibitors. Br. J. Clin. Pharmacol. 72, 581–592. https://doi.org/10.1111/j.1365-2125.2011.03916.x

Li, C.L., Dong, M.H., Ren, Y.J., Li, L.H., 2015. Design, synthesis, biological evaluation and molecular docking of novel dabigatran derivatives as potential thrombin inhibitors. RSC Adv. 5, 23737–23748. https://doi.org/10.1039/c5ra01828e

Pollack, C., Reilly, P., Eikelboom, J., Glund, S., Verhamme, P., A Bernstein, R., Dubiel, R., V Huisman, M., Hylek, E., W Kamphuisen, P., Kreuzer, J., Levy, J., Sellke, F., Stangier, J., Steiner, T., Wang, B., Kam, C.-W., Weitz, J., 2015. Idarucizumab for Dabigatran Reversal, The New England journal of medicine, 73, 511–520. https://doi.org/10.1056/NEJMoa1502000

Ren, W., Ren, Y., Wang, S., 2016. Design, synthesis, anticoagulant activity evaluation and molecular docking studies of a class of N-ethyl dabigatran derivatives, European Journal of Medicinal Chemistry, 120, 148–159. https://doi.org/10.1016/j.ejmech.2016.05.020

Sanford, M., Plosker, G.L., 2008. Dabigatran Etexilate. Drugs, 68, 1699–1709. https://doi.org/10.2165/00003495-200868120-00007

Savelieva, I., Camm, A.J., 2014. Practical considerations for using novel oral anticoagulants in patients with atrial fibrillation. Clin. Cardiol. 37, 32–47. https://doi.org/10.1002/clc.22204

Traynor, K., 2015. Idarucizumab approved for reversal of anticoagulant effects of dabigatran, American Journal of Health-System Pharmacy, 72, 2002–2004.

https://doi.org/10.2146/news150077

Tu, J., Li, J.J., Shan, Z.J., Zhai, H.L., 2017. Exploring the binding mechanism of Heteroaryldihydropyrimidines and Hepatitis B Virus capsid combined 3D-QSAR and molecular dynamics. Antiviral Res. 137, 151–164. https://doi.org/https://doi.org/10.1016/j.antiviral.2016.11.026

Ul-Haq, Z., Khan, N., Zafar, S.K., Moin, S.T., 2016. Active site characterization and structure based 3D-QSAR studies on non-redox type 5-lipoxygenase inhibitors. Eur. J. Pharm. Sci. 88, 26–36. https://doi.org/https://doi.org/10.1016/j.ejps.2016.03.014

Wang, F., Ren, Y.J., Dong, M.H., 2016. Molecular design, synthesis and anticoagulant activity evaluation of fluorinated dabigatran analogues. Bioorganic Med. Chem. 24, 2739–2753. https://doi.org/10.1016/j.bmc.2016.04.038

WEITZ, J.I., BATES, S.M., 2005. New anticoagulants. J. Thromb. Haemost. 3, 1843–1853. https://doi.org/10.1111/j.1538-7836.2005.01374.x

Yang, H., Liu, Q., Gao, X., Ren, Y., Gao, Y., 2017. Novel dabigatran derivatives with a fluorine atom at the C-2 position of the terminal benzene ring: Design, synthesis and anticoagulant activity evaluation. Eur. J. Med. Chem. 126, 799–809. https://doi.org/https://doi.org/10.1016/j.ejmech.2016.12.015